ResearchGate

See discussions, stats, and author profiles for this publication at: https://www.researchgate.net/publication/311734932

First static and dynamic analysis of 3-D-printed sintered ceramics for body armor applications

Article *in* American Ceramic Society Bulletin · January 2017

CITATION
1

READS
88

3 authors, including:



Christopher S Meredith
Army Research Laboratory
18 PUBLICATIONS **136** CITATIONS

SEE PROFILE

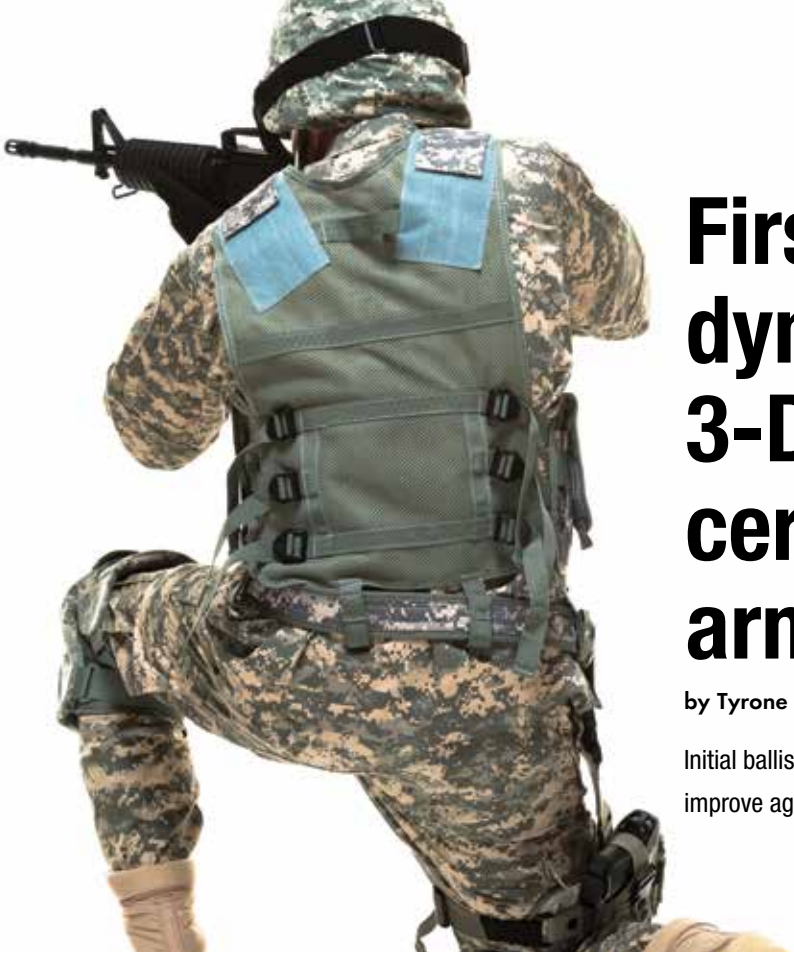
Some of the authors of this publication are also working on these related projects:

Mechanical Behavior of Single Crystal Explosives View project

Compression Strength of Brittle Materials View project

All content following this page was uploaded by Christopher S Meredith on 20 December 2016.

The user has requested enhancement of the downloaded file.



First static and dynamic analysis of 3-D-printed sintered ceramics for body armor applications

by Tyrone L. Jones, Christopher S. Meredith, and Benjamin Becker

Initial ballistic tests show that additive manufacturing is a feasible solution to improve agility, responsiveness, and customization of ceramic armor.

Traditional manufacturing of ceramics used for ballistic impact protection is limited by long lead times, inability to fabricate complex geometries, and expensive components. Ceramic 3-D printing offers engineering-grade components in approximately 90% less time than traditional ceramics manufacturing. Typical turnaround can be days, instead of weeks, depending on the part's complexity. This enables faster time to market and allows for more iterations during the design process, resulting in a better end-product. Additionally, 3-D-printed parts can have a higher degree of complexity for weight reduction while saving on the cost of the part, because less material is required.

The U.S. Army Research Laboratory (Adelphia, Md.) collaborated with HotEnd Works LLC (Oberlin, Ohio) to evaluate the feasibility of producing ceramic armor by 3-D printing. This report examines static and quasi-static parameters (including density, hardness, and fracture strength), semi-infinite penetration performance, and postimpact fracture profiles of 3-D-printed sintered alumina as compared with baseline performance of traditionally sintered alumina.

Although typical U.S. body armor tends to use higher-performance ceramics (such as boron carbide), this program examined 8-mm-thick alumina tiles as the initial, cost-effective material for evaluation of depth of penetration (DOP). Additionally, we used 6-mm- and 8-mm-thick alumina to develop a deeper understanding of the stages of ceramic failure caused by a small steel rod at low-speed impact. We obtained rod-shaped specimens of alumina, nominally 3 mm in diameter and 50 mm in length, to quantify static and quasi-static material properties. The experiments evaluated the following ceramics:

- Traditionally manufactured, sintered alumina AD-995 (also called CAP3) from CoorsTek (Golden, Colo.); and
- 3-D-printed sintered alumina from HotEnd Works (HEW).

Processing 3-D-printed ceramic armor

Manufacturing advanced ceramics typically involves methods such as die pressing or isopressing of ceramic powder that has been combined with binders and plasticizers.[1] To form powder to the desired shape, manufacturers must create tooling that replicates component geometry. If the geometry of a component is beyond a basic shape—such as a rectangle, square, or cylinder—secondary green machining using a computer numerical control mill or lathe is required.

Additive manufacturing of advanced ceramics differs from traditional manufacturing processes mostly in terms of formation of the initial green part. HotEnd Works uses pressurized spray deposition (PSD), which mixes a proprietary blend of advanced ceramic raw material (ceramic powder) with a unique polymeric binder (support material). The polymeric support material serves as a temporary support structure during part formation to accommodate overhangs and other intricate features.[2]

A typical PSD setup deposits materials through high-preci-

Capsule summary

LIMITATIONS

Traditional manufacturing of ceramic armor is limited in time, design, and cost. Additive manufacturing can offer solutions to all of these limitations—but is it feasible?

TAKING A SHOT

A collaboration evaluated the ability to produce 3-D-printed ceramic armor and tested how well these additively manufactured materials held up in ballistic tests.

THE TAKEAWAY

Additive approaches to manufacturing ceramic armor are feasible and offer benefits of customization, improved theater agility, and rapid responsiveness. However, further work is needed to adequately qualify and improve 3-D-printed ceramic armor.

sion deposition nozzles that use mechanical shaping methods to allow patterns of 0.127–3.810 mm in diameter. After the first layer is complete, the process initiates formation of the next layer. Tooling fabrication as well as green machining can be omitted because of the geometric complexity that is possible with PSD.

After forming, the component is thermally debinded followed by densification in a traditional electric or gas furnace. Because shrinkage occurs with additive processing, postprocessing, such as diamond grinding, may be required for components with tight tolerance requirements in terms of flatness or other parameters.

We designed DOP or residual penetration experiments to determine the relative ballistic performance of ceramic materials.[3] DOP testing fires a projectile into a ceramic tile attached to a semi-infinite-thick metal plate, such that the projectile penetrates through the ceramic tile and into the metal plate without deforming the back surface. These experiments avoid the fundamental problem of V_{50} (the velocity at which 50% of a type of projectile is expected to perforate a target) ballistic dependence on armor design (e.g., front-to-back plate ratio and material), require fewer shots than V_{50} tests, and have a sensitivity equivalent to that of other ballistic test methods.[4]

Change in penetration into the metal plates provides a comparison by which to rank performance of ceramic materials. Figure 1 illustrates the target configuration used for these experiments. The target consisted of a 90-mm × 90-mm ceramic tile at a nominal thickness of 8 mm, backed by two aluminum alloy 6061 plates (AA6061, MIL-DTL-32262) with a thickness of 50.8 mm each.[5] We used an epoxy resin (optical aliphatic polyether polyurethane, Dureflex® Grade A4700, Bayer, South Deerfield, Mass.) to attach each tile to the front surface of the first 50.8-mm plate.

We used AA6061 because it is a well-characterized and readily available residual penetration material, and we expected that aluminum plates would provide better resolution than steel backer plates. We used no cover plates.

We conducted three ballistic impact experiments for each alumina manufacturing process at the U.S. Army Research Laboratory. Tests used projectiles of copper-jacketed 12.7 mm APM2, which includes a hardened steel core penetrator with a length of 47.6 mm, a diameter of 10.87 mm, and an aspect ratio of 4. Projectiles had a nominal weight of 46 g and core density of 7.85 g/cm^3.

Ballistic tests used a nominal impact velocity of 848 m/s, although some shots varied from 824 to 872 m/s. This variability could result from interior barrel conditions, variations in APM2 material properties, or gun operator influence, such as projectile powder measurements. We intentionally chose this impact velocity to produce a range of measureable residual penetrations while being consistent with real-world ballistic impact conditions. The schematic in Figure 2 shows how residual penetration was measured.[3]

We performed additional experiments with a high-speed camera to qualitatively assess fracture propagation of the alumina caused by low-speed impact by a small rod-shaped projectile. These

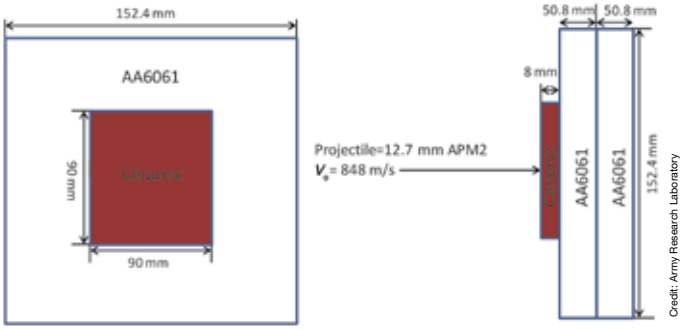


Figure 1. Sketch and dimensions of ceramic laminate.

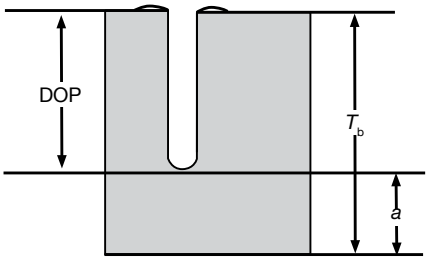


Figure 2. Strategy for measurement of residual penetration in ballistic tests. Measurement of *a* avoided errors that could be caused by deformation of the aluminum block around the cavity entrance.[6]

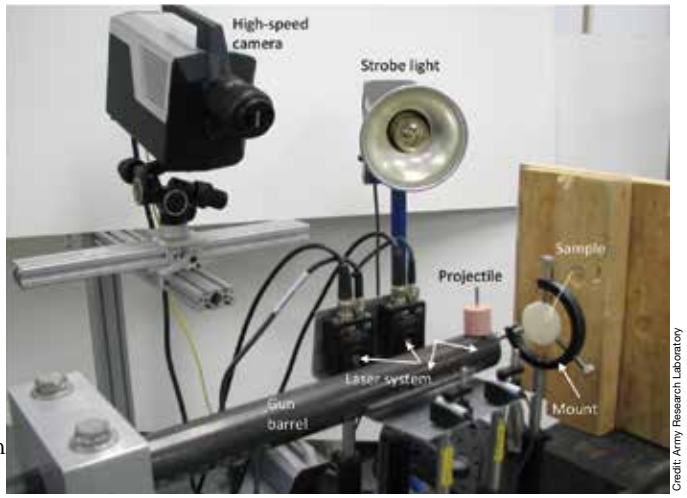
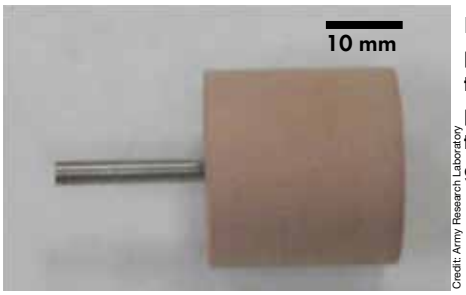
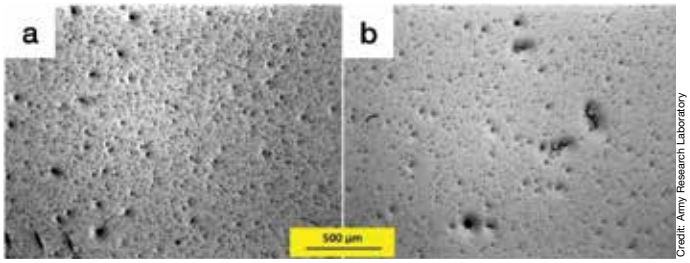


Figure 3. Experimental setup for recording fracture of samples during ballistic tests.



Credit: Army Research Laboratory

Figure 4. A rod projectile attached to a sabot, which properly positioned the rod within the gun barrel.



Credit: Army Research Laboratory

Figure 5. Representative microstructure of (a) CoorsTek AD-995 manufactured by isopressing and sintering and (b) HotEnd Works alumina manufactured by pressurized spray deposition and sintering.



Credit: Army Research Laboratory

Figure 6. Residual penetrator after impact of shot No. 13159 against CoorsTek alumina AD-995.



Credit: Army Research Laboratory

Figure 7. Residual penetrator after impact of shot No. 13161 against HotEnd Works alumina.

experiments impacted 6- and 8-mm-thick tiles at approximately 210 m/s because of limitations of the gas gun. Thus, direct comparisons with ballistic tests may be dubious.

Figure 3 shows the experimental setup. The gun fired a right-circular-cylinder steel-rod projectile with a diameter of 3.18 mm and a length of 35 mm, which was connected to a machinable foam sabot that held the rod as it accelerated down the larger-diameter gun barrel (Figure 4). The projectile, made of hardened M2 steel with a Rockwell C (R_C) hardness of 62, weighed 7.5 g, including the weight of the sabot. The projectile hardness was similar to that of an APM2 projectile.

Table 1. Properties of CoorsTek and HotEnd Works alumina samples

Material	Density (g/cm³)	Flexure strength (MPa)	Knoop hardness (GPa)
CoorsTek AD-995	3.92 ± 0.00	162 ± 54	13.2 ± 1.3
HotEnd Works	3.89 ± 0.08	130 ± 38	14.7 ± 1.0

Comparison of performance of HotEnd Works 3-D-printed alumina with CoorsTek AD-995

Prior to examining ballistic behavior, we determined density, hardness, quasi-static flexural strength, and microstructure of each rod-shaped alumina specimen, nominally 3 mm in diameter and 50 mm in length. The Archimedes method provided density determinations, ASTM C1684 guidelines determined flexure strength,[7] and ASTM C1326 guidelines determined Knoop Hardness at 2,000 g.[8] Table 1 summarizes these data. Figure 5 shows microstructure of each alumina sample.

Alumina materials appeared similar based on these properties. The CoorsTek sample had seemingly higher pore density, but the HotEnd Works sample had larger maximum pore size, with some cracks connecting neighboring pores. The HotEnd Works alumina was 0.03 ± 0.08 g/cm³ less dense than the CoorsTek alumina.

We fired a few shots into monolithic AA6061 plates at velocities of 824–872 m/s to quantify DOP without the ceramic.[9] Deceleration was the primary penetrator defeat mechanism of AA6061 over the velocity regime. We then measured residual penetration values and plotted them as a function of striking velocity to produce a baseline curve. Linear regression of the reference data yielded the following equation:

$$\text{DOP} = 0.1959V_{\text{X-ray}} - 84.406 \qquad (1)$$

where $V_{\text{X-ray}}$ is striking velocity quantified using X-ray measurements. A square of the correlation coefficient (R^2) of 0.946 indicates that this curve is a reasonable approximation. For example, an experimental impact velocity of 848 m/s would be expected to result in a DOP of 81.73 mm. For these experiments, this is the DOP baseline for AA6061.

As previously described, we fabricated ceramic target assemblies for all materials. In general, we evaluated three tiles of equal thickness (or areal density) for each material. To adjust for variations in the actual strike velocity, we normalized all residual penetration values to a striking velocity of 848 m/s based on the empirical fit shown in Eq. (1). The correction was made as follows:

$$\text{Corrected DOP} = \text{Measured DOP} + [0.1959(848 - V_{\text{X-ray}})] \qquad (2)$$

This technique is valid provided that a significant amount of the penetrator reaches the backup plate, the correction is relatively small, and the penetrator defeat mechanism has not significantly changed with velocity.[9] In support of this assumption, observations of the size and shape of impact showed no significant differences in penetrator cavity for impact velocity variations.

We obtained data for alumina tiles at a nominal thickness of 8 mm. Table 2 lists ballistic impact measurements. We measured an average DOP with correction of 14.43 mm with a standard deviation of 3.01 mm for CoorsTek AD-995. We measured an average DOP with correction of 24.01 mm with a standard deviation of 2.06 mm for HotEnd Works alumina. The difference between HotEnd Works and CoorsTek aluminas, 9.58 mm, is equivalent to about three-quarters of the projectile diameter or one-sixth of the projectile length.

In these limited experiments, CoorsTek AD-995 tiles caused

Table 2. Ballistic impact measurements for alumina tiles

Shot No.	Alumina type	Striking velocity (m/s)	Pitch (deg)	Yaw (deg)	Total yaw (deg)	DOP (mm)	DOP_{corr} (mm)
13157	CoorsTek	840	0.47	–0.62	0.78	16.00	17.56
13158	CoorsTek	843	0.61	–0.39	0.72	13.21	14.18
13159	CoorsTek	846	0.26	–0.48	0.54	11.18	11.56
13160	HotEnd Works	860	0.51	–0.50	0.72	28.70	26.34
13161	HotEnd Works	850	0.31	–0.58	0.65	23.62	23.22
13162	HotEnd Works	850	0.32	–0.46	0.56	22.86	22.46

more damage to the penetrator than HotEnd Works alumina tiles. Interestingly, the DOP for each ceramic laminate increased as yaw increased. More experiments are needed to determine if this response is a coincidence or a phenomena.

The penetrator underwent two failure mechanisms, fragmentation and erosion, when it impacted Coorkstek AD-995 tiles (Figure 6). However, the penetrator underwent only erosion when it impacted HotEnd Works alumina tiles (Figure 7).

We measured recovered residual projectile cores and calculated curve fits for these data (Figures 8 and 9), although it is unlikely that all debris was recovered because projectiles shattered and eroded on impact. Nonetheless, we measured length of the largest piece as the residual penetrator length. We did not measure length of shot No. 13159 because only small fragments of the projectile were recovered. However, we did measure mass of these recovered core fragments. The unaltered core was added to the figure as a point of reference at the striking velocity of 825 m/s.

We optically examined postexperimental targets for ceramic failure analysis. CoorsTek and HotEnd Works alumina began failing with tensile fracture, then continued into comminution to dissipate energy of the penetrator. Both types of alumina exhibited similar extents of ceramic damage. Typical ceramic failures are shown in Figures 10 and 11. However, the DOP cavity profile into AA6061 plates distinctly differed.

During ballistic impact, CoorsTek AD-995 alumina typically fractured the penetrator into two large pieces and some small chips before starting the erosion process. As a result, the AA6061 plate contained two projectile canals. The HotEnd Works alumina did not fracture but eroded only the penetrator. As a result, the HotEnd Works plate contained one residual penetrator canal.

Because this study used AA6061 as the reference material, Eq. (3) provided a coefficient of performance (C_p) of the ceramics compared with the reference material:

$$C_p = \left(\frac{}{AA6061}\right)\frac{DOP_{Base_AA6061}}{AD_{Ceramic}}\frac{DOP_{Corr_AA6061}}{} \quad (3)$$

where DOP_{Base_AA6061} is the average expected residual depth of penetration into bare aluminum at 848 m/s; DOP_{Corr_AA6061} is the residual DOP into AA6061 after perforating the ceramic tile, corrected for variations in striking velocity; and $AD_{ceramic}$ is the areal density of the ceramic. In these tests, DOP_{Base_AA6061} was 81.73 mm, $AD_{AD\text{-}995}$ was 31.36 kg/m^2, $AD_{HEW_Alumina}$ was 31.12 kg/m^2, and ρ_{AA6061} was 2.70 g/cm^3.

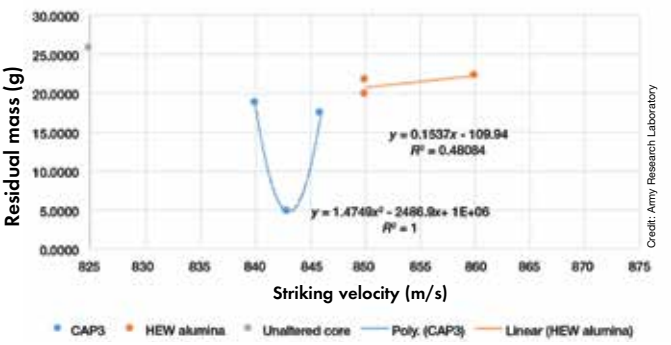


Figure 8. Analysis of residual penetrator with residual penetrator mass of 12.7-mm APM2 into AA6061 as a function of striking velocity.

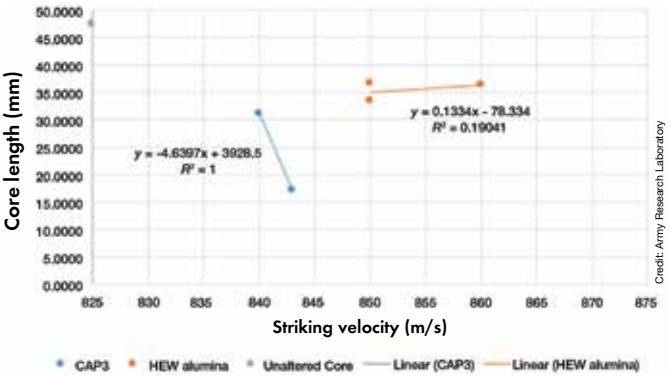


Figure 9. Analysis of residual penetrator with residual penetrator length of 12.7-mm APM2 into AA6061 as a function of striking velocity.



Figure 10. CoorsTek AD-995 alumina tile after impact. The left image shows the complete sample, whereas the right displays a cross section of the same sample.



Figure 11. HotEnd Works alumina tile after impact. The left image shows the complete sample, whereas the right displays a cross section of the same sample.

For each alumina sample, we calculated a C_p value, which provides a relative comparison of the ceramic with AA6061 (i.e., a C_p of 5 means the ceramic is 5 times more weight-effective than AA6061) (Table 3). Figure 12 illustrates a ceramic performance map, which clearly shows that CoorsTek alumina has superior performance than HotEnd Works alumina.

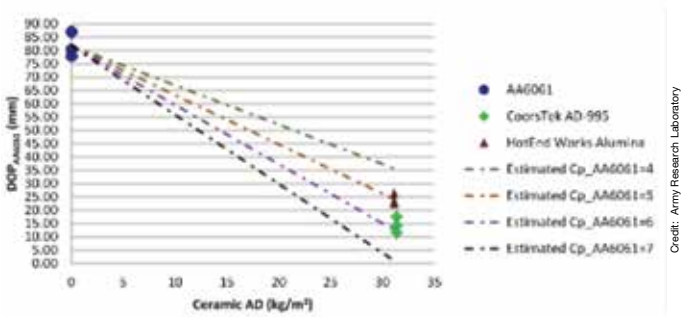


Figure 12. Ceramic performance map comparing AA6061, CoorsTek AD-995, and HotEnd Works alumina samples.

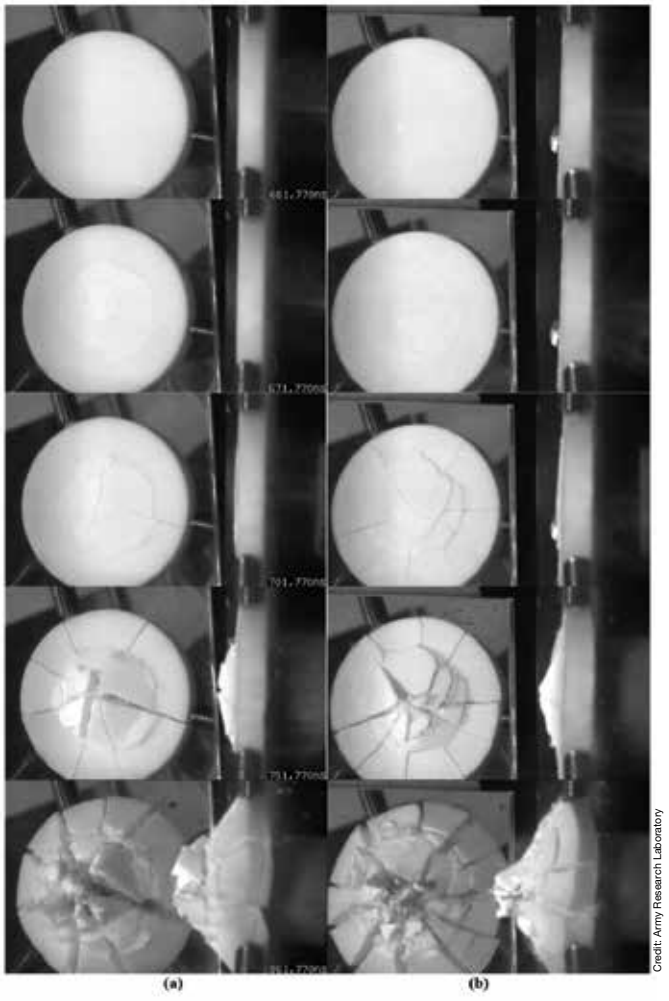


Figure 13. Progressive fracture of 6-mm alumina samples from (a) CoorsTek and (b) HotEnd Works.

Table 3. Comparative performance of ceramics

Experiment	Coefficient of performance (C_p)	
	CoorsTek AD-995	HotEnd Works alumina
1	5.52	4.81
2	5.82	5.08
3	6.04	5.14

Figure 13 shows progressive failure through brittle fracture of the 6-mm-thick ceramic samples with no backing plate. CoorsTek and HotEnd Works alumina samples

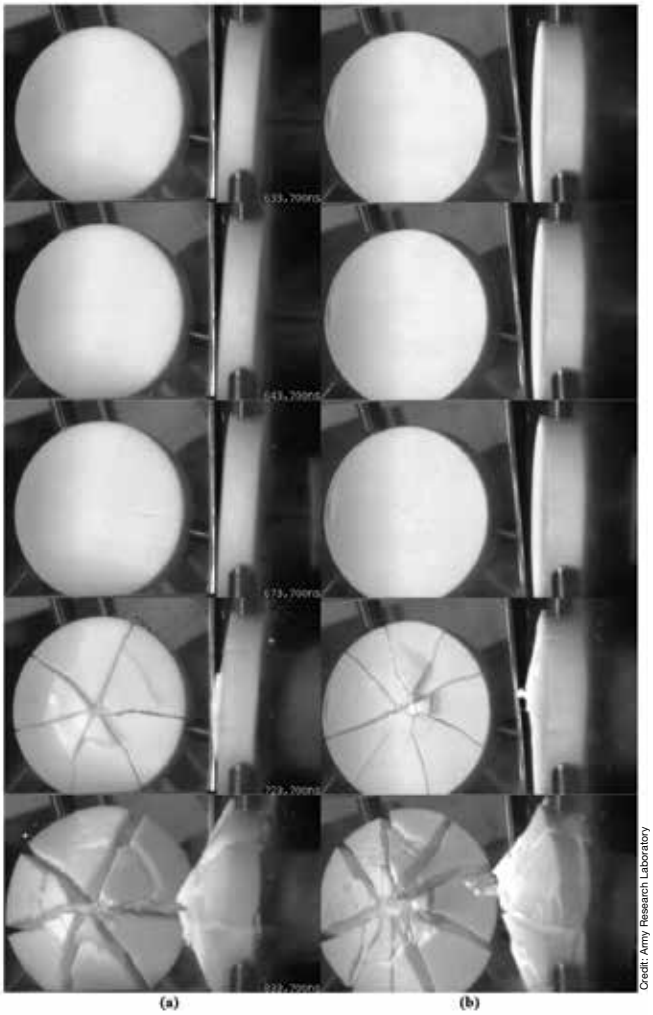


Figure 14. Progressive fracture of 8-mm alumina samples from (a) CoorsTek and (b) HotEnd Works.

underwent projectile velocities of 206 and 214 m/s, respectively. The series of images shows the samples immediately before impact and 10, 40, 90, and 200 μs after impact. The samples showed similar overall features—concentric cracks first appear several microseconds after impact, and then radial cracks appear.

Concentric cracks at the back face probably form a cone crack through the thickness of the sample, but it cannot be seen because the alumina is opaque. After 90 μs, concentric cracks have clearly coalesced, because the rod has pushed out inner material to a greater extent than material near the outer edge. At 200 μs, the samples appear similar, although the HotEnd Works alumina is slightly more fragmented.

The biggest difference between the two materials is that the CoorsTek sample has less radial cracks than the HotEnd Works 3-D printed sample. Additionally, the area within concentric cracks of the HotEnd Works alumina has further cracked and started to break up after 90 μs, whereas the same region of the CoorsTek alumina shows no further cracks. Table 4 shows a summary of the dynamic failure modes.

Figures 13 and 14 show failure progression of 6- and 8-mm-thick samples, respectively, with projectile velocities of 216 and

224 m/s immediately before impact and 10, 40, 90, and 200 µs after impact. As before, the two alumina samples display overall similar features. The 8-mm-thick samples show very few concentric cracks following impact, and radial cracks are the first damage to appear.

As expected, it takes longer for cracks to emerge on the backside of samples, and thicker samples have less damage at the same time after impact. In addition, the CoorsTek alumina has fewer radial cracks than the HotEnd Works alumina sample. At a couple hundred microseconds after impact, the HotEnd Works alumina shows greater fragmentation. Table 5 shows a summary of the dynamic failure modes.

Future armor

This program was a preliminary investigation into the viability of using a 3-D-printed alumina ceramic for body armor applications. Initial results show the feasibility of additive approaches to manufacturing ceramic armor, which could lead to customized armor for soldiers, vehicles, and equipment. In addition, additive manufacturing of armor in the field could improve theater agility and responsiveness.

However, although the results show feasibility, they also point to further work that needs to be done. Specifically, the coefficient of performance showed that CoorsTek alumina AD-995 was 13% more efficient against ballistic penetration than HotEnd Works 3-D-printed alumina tiles. The low-velocity, rod-impact experiments into unbacked ceramic disks provide initial clues as to why.

These exploratory experiments show there is a critical thickness limit at a given velocity that is needed to simulate the realistic failure modes of the alumina ceramic under ballistic impact. In 6-mm-thick ceramic tiles, the rod impact exhibited more plugging mode failure, which is not desirable in conventional armor. In 8-mm-thick ceramic tiles, the HotEnd Works alumina had a greater number of radial cracks and fragmented to a greater extent than the CoorsTek alumina. Further, the disk diameters were adequate for low-velocity rod impact.

Next, the 3-D deposition process needs to be improved to reduce pore size and increase flexural strength of the 3-D-printed ceramic material. Improvements to the sintering method will be the critical correlation to improve ceramic failure mechanisms and penetrator failure mechanisms during low-velocity rod impacts and ballistic penetrator impacts.

Further, Hugoniot shock pressure limit experiments are imperative. At pressures just above the elastic limit—called the Hugoniot elastic limit (HEL)—a shock wave is split into a two-wave structure by the HEL, which is determined by strength.[10] Up to the HEL, a single, elastic, supersonic shock wave propagates. At higher pressures, shock compression causes plastic deformation as well.

A solid just above its HEL is softer (i.e., more compressible) than it is below its HEL. By measuring time-resolved shockwave profiles, we can derive HELs, mechanical constitutive properties, and equations of state,[10] which then allow us to analytically predict quantification of the fracture behavior between ceramics manufactured by various methods. Successful implementation of these steps, including initial correlation between these dynamic variables and manufacturing process variables, are expected to elevate the 3-D-printed ceramic static, quasi-static, and dynamic properties to match, or exceed, those of conventionally sintered alumina. ■

Acknowledgements

The authors acknowledge assistance from Jeffrey Swab in characterization of the initial material properties.

About the authors

Tyrone L. Jones and Christopher S. Meredith are with the Weapons and Materials Research Directorate at the U.S. Army Research Laboratory (Adelphia, Md.). Benjamin Becker is with HotEnd Works LLC (Oberlin, Ohio). Contact Becker at benjamin.becker@hotendworks.com.

References

[1]A. King, *Ceramic technology and processing*, 1st ed. William Andrew Publishing, Norwich, N.Y., 2002.

[2]B. Becker, "Additive changes to advanced ceramics," *Ceram. Ind.*, Apr. 10, 2014 (accessed May 10, 2016) http://www.ceramicindustry.com/articles /93848-additive-changes-to-advanced-ceramics.

[3]P. Woolsey, D. Kokidko, and S. Mariano, "Alternative test methodology for ballistic performance ranking of armor ceramics," Report No. MTL-TR 89-43, Army Materials Technology Laboratory, Watertown, Mass., 1989.

[4]"V50 ballistic test for armor," Report No. MIL-STD-662F, Army Research Laboratory, Aberdeen Proving Ground, Md., Dec. 18, 1997.

[5]"Armor plate, aluminum alloy, unweldable applique 6061," Report No. MIL-DTL-32262, Army Research Laboratory, Aberdeen Proving Ground, Md., July 2007.

[6]T. Jones, "Investigation of the kinetic energy characterization of advanced ceramics," Report No. ARL-TR-7263, Army Research Laboratory, Aberdeen Proving Ground, Md., April 2015.

[7]ASTM C1684, "Standard test method for flexural strength of advanced ceramics at ambient temperature-cylindrical rod strength," ASTM International, West Conshohocken, Pa., 2008.

[8]ASTM C1326, "Standard test method for Knoop indentation hardness of advanced ceramics," ASTM International, West Conshohocken, Pa., 2013.

[9]T. Jones, "Investigation of the kinetic energy characterization of advanced ceramics," Report No. ARL-TR-7263, Army Research Laboratory, Aberdeen Proving Ground, Md., April 2015.

[10]W.J. Nellis, "Dynamic compression of materials: Metallization of fluid hydrogen at high pressures," *Rep. Prog. Phys.*, **69** [5] 1479 (2006). ■

Table 4. Dynamic failure modes of 6-mm-thick alumina disks

Time interval (µs)	CoorsTek AD-995	HotEnd Works 3-D printed alumina
Preimpact, 0	Disk intact	Disk intact
Postimpact, 10	Radial-forming cracks	Radial-forming cracks
Postimpact, 40	Longitudinal cracks forming	Longitudinal cracks forming
Postimpact, 90	Seven longitudinal cracks that run from center to edge of disk; plugging with discrete fragments forming	Nine longitudinal cracks that run from center to edge of disk; plugging with comminution process beginning
Postimpact, 200	Fragmentation process is converting to comminution process	Comminution process is occurring

Table 5. Dynamic failure modes of 8-mm-thick alumina disks

Time interval (µs)	CoorsTek AD-995	HotEnd Works 3-D printed alumina
Preimpact, 0	Disk intact	Disk intact
Postimpact, 10	Disk intact	Disk intact
Postimpact, 40	Longitudinal cracks forming	Longitudinal cracks forming
Postimpact, 90	Six longitudinal cracks that run from center to edge of disk; plugging mode beginning; discrete fragments forming	Eight longitudinal cracks that run from center to edge of disk; no plugging mode; comminution process is beginning
Postimpact, 200	Fragmentation process is transforming into comminution process	Comminution process is occurring

View publication stats